NeuroImage: Clinical 24 (2019) 102002

Contents lists available at ScienceDirect

NeuroImage: Clinical

journal homepage: www.elsevier.com/locate/ynicl

Magnetic resonance imaging of the cervical spinal cord in spinal muscular atrophy

Marloes Stam[a,1], Wieke Haakma[b,1], Lidy Kuster[b], Martijn Froeling[b], Marielle E.P. Philippens[c], Clemens Bos[b], Alexander Leemans[d], Louise A.M. Otto[a], Leonard H. van den Berg[a], Jeroen Hendrikse[b,1], W. Ludo van der Pol[a,*,1]

[a] UMC Utrecht Brain Center, Department of Neurology, University Medical Center Utrecht, Utrecht University, Utrecht, The Netherlands
[b] Department of Radiology, University Medical Center Utrecht, Utrecht University, Utrecht, The Netherlands
[c] Department of Radiotherapy, Cancer Center, University Medical Center Utrecht, Utrecht University, Utrecht, The Netherlands
[d] Image Sciences Institute, University Medical Center Utrecht, Utrecht, The Netherlands

ARTICLE INFO

Keywords:
Spinal muscular atrophy
SMA
MRI
DTI
Spinal cord
Nerve roots

ABSTRACT

Objective: In this study we investigated the potential value of magnetic resonance imaging (MRI) and diffusion tensor imaging (DTI) in characterizing changes in the cervical spinal cord and peripheral nerve roots in vivo in patients with spinal muscular atrophy (SMA).
Methods: We developed an MRI protocol with 4 sequences to investigate the cervical spinal cord and nerve roots on a 3 Tesla MRI system. We used 2 anatomical MRI sequences to investigate cross-sectional area (CSA) at each spinal segment and the diameter of ventral and dorsal nerve roots, and two diffusion tensor imaging (DTI) techniques to estimate the fractional anisotropy (FA), mean (MD), axial (AD) and radial diffusivity (RD) in 10 SMA patients and 20 healthy controls.
Results: There were no significant differences in CSA ($p > .1$), although an 8.5% reduction of CSA in patients compared to healthy controls was apparent at segment C7. DTI data showed a higher AD in grey matter of patients compared to healthy controls ($p = .033$). Significantly lower MD, AD and RD values were found in rostral nerve roots (C3-C5) in patients ($p < .045$).
Conclusions: We showed feasibility of an advanced 3 T MRI protocol that allowed differences to be determined between patients and healthy controls, confirming the potential of this technique to assess pathological mechanisms in SMA. After further development and confirmation of findings in a larger sample, these techniques may be used to study disease course of SMA in vivo and evaluate response to survival motor neuron (SMN) augmenting therapy.

1. Introduction

Hereditary proximal spinal muscular atrophy (SMA) is characterized by dysfunction and degeneration of motor neurons in the anterior horn of the spinal cord and is caused by survival motor neuron (SMN) protein deficiency due to a homozygous loss of function of the SMN1 gene (Lunn and Wang, 2008). The SMN protein has generic and tissue-specific functions, including pre-mRNA splicing (Pellizzoni et al., 1998) and axonal transport of mRNA (Fallini et al., 2012; Dale et al., 2011).

Alterations in the anatomy of the spinal cord and nerve roots of patients with SMA were part of the earliest descriptions of SMA, but have only been documented post-mortem and therefore represent late-stage disease phenomena (Harding et al., 2015; Araki et al., 2003). Animal models of SMA have allowed insight into the development of pathology (Kariya et al., 2008). However, additional techniques are needed to elucidate the mechanisms in vivo that underlie SMA pathogenesis and which can monitor the response to recently introduced SMN protein augmenting therapies at an early stage (Sumner and Crawford TO, 2018) as the execution of clinical trials in SMA is complicated by the lack of sensitive outcome measures (Bertini et al., 2005).

Magnetic resonance imaging (MRI) can provide potential biomarkers for SMA. It has been used to assess muscle volume and fat

* Corresponding author at: UMC Utrecht Brain Center, Department of Neurology F02.230, University Medical Center Utrecht, Heidelberglaan 100, 3508 GA Utrecht, The Netherlands.
E-mail address: W.L.vanderPol@umcutrecht.nl (W.L. van der Pol).
[1] These authors contributed equally to the manuscript.

https://doi.org/10.1016/j.nicl.2019.102002
Received 7 June 2019; Received in revised form 23 August 2019; Accepted 2 September 2019
Available online 03 September 2019

Table 1
MRI acquisition parameters.

Sequence name	DTI in-plane	mFFE	DTI isotropic	T2-FFE
Plane	Axial	Axial	Coronal	Axial
TE (ms)	96	TE1 = 7.8 (ΔTE = 9)	62	6
TR (ms)	1657	700	6441	12
NSA	10	2	1	1
Field of view (mm^2)	240 × 240	160 × 160	280 × 280	200 × 200
Acquisition matrix	256 × 256	560 × 560	112 × 112	432 × 432
Voxel size (mm^3)	0.94 × 0.94 × 5.0	0.29 × 0.29 × 5.0	2.5 × 2.5 × 2.5	0.46 × 0.46 × 0.5
Slices	10	17	30	160
b-value (s/mm^2)	100, 800	–	100, 800	–
Number of gradient directions	10, 10	–	3, 10	–
Acquisition time	5:50	5:47	10:05	5:46
Bandwidth (Hz)	rBW: 881 EPI BW: 10.8	rBW: 144	rBW: 3149 EPI BW: 54.1	rBW: 144

Abbreviations: MRI: magnetic resonance imaging; DTI: diffusion tensor imaging; mFFE: multi echo T2* weighted gradient echo; T2-FFE: T2* weighted gradient echo; TE: echo time; TR: repetition time; NSA: number of signal averages; rBW: receiver bandwidth; EPI: Echo Planar Imaging.

fraction of the upper and lower extremities (Sproule et al., 2011; Durmus et al., 2017) and spinal cord atrophy (El Mendili et al., 2016; Querin et al., 2018). Diffusion tensor imaging (DTI), an MRI technique that is sensitive to the random motion of water molecules, can provide additional information on the microstructural organization and status of nervous tissue. DTI has previously been applied in the brain (Querin et al., 2018; Müller et al., 2016), muscle structures (Oudeman et al., 2016), peripheral nerves (Haakma et al., 2017) and the spinal cord (Toosy et al., 2014) in neuromuscular diseases, including one recent study in SMA, assessing the corticospinal tract in the brain and corticospinal tracts and dorsal columns in the spinal cord (Querin et al., 2018). In this study we investigated the potential value of MRI and DTI in characterizing changes in the cervical spinal cord and peripheral nerve roots in vivo in SMA patients. We hypothesize that due to pathological changes in SMA there will be a change in the cross-sectional area (CSA) and DTI parameters of the cervical spinal cord and nerve roots.

2. Methods

2.1. Participants

We recruited 10 patients with a genetically confirmed diagnosis of SMA type 2 or 3, aged 12 years and older from the national SMA registry at the University Medical Center Utrecht in the Netherlands, a tertiary referral center for SMA. We used the definition of SMA type established by the 1992 SMA consortium meeting (Munsat and Davies, 1992) (i.e. type 2: onset between 6 and 18 months, never able to walk; type 3: onset between 18 months and 30 years, able to walk at some stage in life) with a further delineation of SMA type 3a and 3b based on age at symptom onset before or after 3 years of age (Zerres and Schöneborn, 1995). All eligible patients in the registry were invited to participate to minimize bias. For each patient, two age- and gender-matched healthy controls were included without history of neuropathy or neuromuscular complaints, to adjust for age- and gender-related changes in MRI parameters (Taso et al., 2016). Exclusion criteria were: signs of nocturnal hypoventilation (i.e. recurrent morning headaches, night sweats, orthopnea), tracheostomy, any type of (non-)invasive ventilation, pronounced swallowing disorders, a postural change of > 15% in forced vital capacity between sitting and supine position, previous trauma or surgery of the (cervical) spinal cord, and any contra-indication for MRI.

2.2. Ethics statement

The Medical Ethics Review Committee (MERC) of the University Medical Center Utrecht approved the study protocol. Written informed consent was obtained from all participants and from parents or legal guardians of participants younger than 18 years. The study was carried out in accordance with the Declaration of Helsinki (latest version WMA General Assembly 2013, Fortaleza, Brazil).

2.3. Clinical outcome measures

We used the Medical Research Council (MRC) scale to assess strength of muscles innervated by C5-C8 roots (MRC and Medical Research Council, 1976). We examined the biceps, triceps, infra- and supraspinatus, pectoralis major, deltoid muscles, wrist flexors and extensors and finger flexors, extensors and abductors. Motor function was evaluated using the Hammersmith Functional Motor Scale Expanded (HFMSE), a 33-item test of motor function developed to evaluate motor performance in patients with SMA types 2 and 3 (O'Hagen et al., 2007). We recorded the participant's weight and height, since this could potentially influence anatomical measures of the spinal cord. We determined SMN2 copy numbers using Multiplex Ligation-dependent Probe Amplification (MLPA) analysis (SALSA MLPA kit P060 version B2; www.mlpa.com; www.mrcholland.com) (Wadman et al., 2017).

2.4. MRI protocol and data acquisition

All subjects were scanned on a 3 Tesla MRI system (Ingenia, Philips Healthcare, Best, the Netherlands) with a neurovascular 15-channel surface coil. Two different areas in the cervical spine were evaluated using 4 different MRI sequences: 1) the cervical spinal cord (spinal segments C4-C8) with a multi echo T2* weighted gradient echo (= multi-echo steady state free precession = mFFE) sequence and a "high in-plane" resolution DTI scan, and 2) the cervical peripheral nerves (spinal segments C3-C8) with a T2* weighted gradient echo (T2-FFE) sequence and an "isotropic" resolution DTI scan. Both DTI scans were obtained using b = 100 s/mm^2 (b100) and b = 800 s/mm^2 (b800) to decrease the influence of cerebral spinal fluid. Table 1 displays the acquisition parameters of the MRI sequences.

2.5. Data processing

Before processing, all data were inspected visually for overall image quality and artifacts (Tournier et al., 2011). Both DTI acquisitions were processed identically using ExploreDTI (www.ExploreDTI.com) (Leemans et al., 2009) consisting of the following steps. First the b100 images were registered, then the b800 images were registered to the mean of the registered b100. Images were corrected for eddy current induced distortions, subject motion, and susceptibility artifacts (Leemans and Jones, 2009; Irfanoglu et al., 2012). Next, tensors were fitted with the iteratively weighted linear least squares procedure

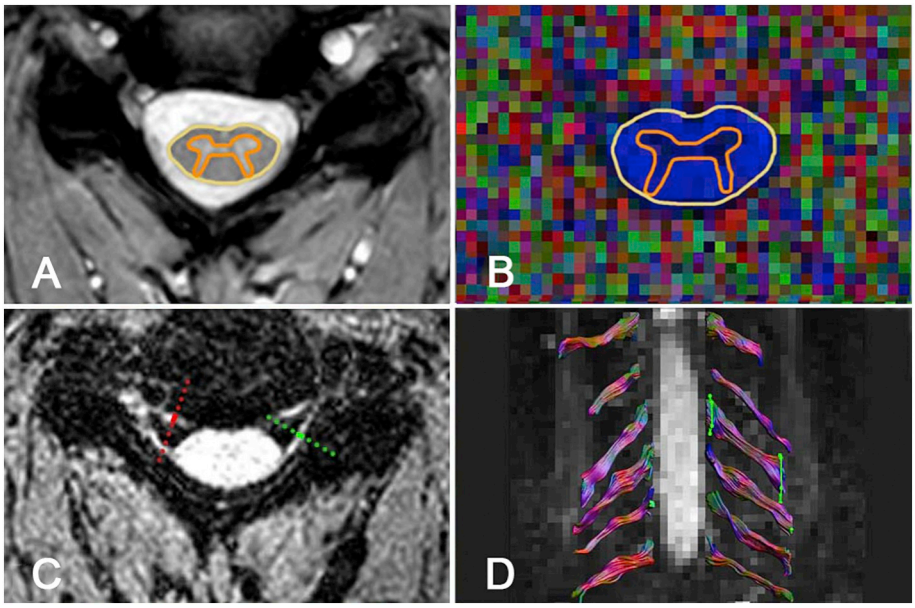

Fig. 1. Data acquisition.
A) Delineation of the grey (orange line) and white matter (yellow line) on the multi echo T2* weighted gradient echo (mFFE) and B) on the "high in-plane" resolution diffusion tensor imaging (DTI) scan. C) The dotted lines on the T2* weighted gradient echo (T2-FFE) scan indicate where the diameter of the nerves is measured perpendicular to the nerve. The green line is positioned on the dorsal and the red line on the ventral nerve root. D) Fiber tractography of the cervical nerve roots from the "isotropic" resolution DTI scan showing two 'AND' ROIs indicating the segment that was used for analysis.

(Veraart et al., 2013). To visualize the nerves and extract the diffusion properties, fiber tractography (FT) was used. Fiber tracts were reconstructed by applying whole volume FT with a fractional anisotropy (FA) threshold of 0.1, minimum fiber length of 15 mm, and maximum fiber angle change per 1 mm step of 30° for both DTI scans. Average diffusion values for each nerve segment were calculated using a tract-based analysis with manually drawn regions of interest (ROIs) to select the appropriate nerve segments.

2.5.1. Spinal cord

2.5.1.1. Cross-sectional area of the cervical spinal cord. Fig. 1A shows an example of how we delineated CSA of the whole spinal cord (spinal segments C4-C8) and grey matter (spinal segments C5-C7) at each segment where the nerve root branched with the spinal cord on the multi echo T2* weighted gradient echo (mFFE) scan. The white matter CSA was calculated by subtracting the grey matter from the whole spinal cord CSA. We calculated spinal cord atrophy at each segment by expressing the mean difference of CSA between patients and matched controls (controls – patients) as a percentage of the mean of the control.

2.5.1.2. Microstructural properties of the cervical spinal cord. In the "high in-plane" resolution DTI scan we manually segmented the grey matter, white matter, and whole spinal cord at spinal segments C5-C7 (Fig. 1B). We used 4 diffusion parameters to investigate the microstructural properties of nervous tissue: the FA which approaches 1 when diffusion is predominantly oriented in one direction, the mean diffusion (MD) which is the average of three eigenvalues (i.e. the length of the diffusion in a specific orientation), the axial diffusivity (AD) which is equal to the largest eigenvalue, and the radial diffusivity (RD) which is the average of the second and third eigenvalues (Fig. 2). Estimates for the FA, MD, AD and RD were calculated for the grey matter, white matter, and whole spinal cord.

2.5.2. Cervical nerve roots

2.5.2.1. Thickness of the ventral and dorsal nerve roots. We measured the diameter of the ventral and dorsal nerve roots on both sides on the T2* weighted gradient echo (T2-FFE), halfway between where the ventral and dorsal nerve roots branch with the spinal cord and where they merge, as displayed in Fig. 1C.

2.5.2.2. Microstructural properties of the cervical peripheral nerve roots. We reconstructed the nerves at spinal segments C3-C8 with the

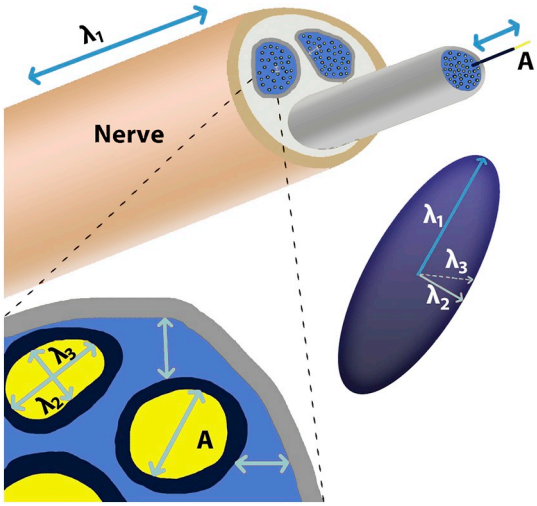

Fig. 2. Schematic explanation of diffusion tensor parameters.
The main diffusion parameters are calculated from the three eigenvalues λ_1, λ_2, and λ_3: The mean diffusivity (MD) is the average of λ_1, λ_2, and λ_3.The largest eigenvalue, λ_1, is the axial diffusivity (AD) which represents the diffusivity along the main axis. The diffusion perpendicular to the nerve is the radial diffusivity (RD), which is the average of λ_2 and λ_3. Fractional anisotropy (FA) represents the degree in which diffusion is oriented in one direction. 'A' represents the axon.

data obtained with the "isotropic" resolution DTI scan. Segments of 3 cm of C3-C8 nerve roots were selected where the nerve branched with the spinal cord, as described by Haakma et al. (2016)). In short, 'SEED', 'AND', and 'NOT' ROIs were used to reconstruct the fiber tracts. For each segment, estimates for the FA MD, AD, and RD were computed (Fig. 1D).

2.6. Data analysis

Statistical analyses of the obtained parameters were performed in IBM SPSS Statistics (version 24; IBM Corp., Armonk, N.Y., USA). We used a mixed analysis of covariance (ANCOVA) with random intercept for the outcome measure as dependent variable and 'segment', 'gender', and 'participant group' as covariates. Fixed effects for the analyses of outcome measures of the "high in-plane" resolution DTI scan and mFFE

scan were 'segment', 'gender', 'participant group' and the interaction of 'segment' and 'participant group'. For the outcome measures of the "isotropic" resolution DTI scan the variable 'side' was added to the model as a covariate and fixed effect. Distribution was tested with a Kolmogorov-Smirnov test. We assessed correlations between MRI parameters and clinical scores with Spearman's rank correlation coefficient. We exclusively performed analyses of correlation with clinical scores in patients and only for MRI parameters that were found to be significantly different between patients and controls. For all statistical analyses we considered a p-value of < 0.05 to be significant.

The sample size was not calculated prospectively, because of the unpredictable effect size. Sample size was determined by the number of eligible patients willing to participate.

3. Results

3.1. Patients

Initially, we included 10 patients with SMA and 20 gender- and age-matched healthy controls. After visual inspection of the imaging data, 2 patients were excluded because of low image quality due to motion artifacts, which made the entire MRI dataset unusable for analysis. We therefore recruited 2 additional patients. Participant characteristics are summarized in Table 2.

3.2. Spinal cord

3.2.1. Cross-sectional area of the cervical spinal cord

We were able to measure CSA of the whole spinal cord (white and grey matter combined) successfully at segments C4 in 8 patients and 16 controls, at C5 in 5 patients and 18 controls, at C6 in 5 patients and 18 controls, at C7 in 5 patients and 17 controls, and at C8 in 4 patients and 13 controls. Missing values were mainly caused by motion artifacts. We could distinguish grey matter CSA from white matter CSA in 4 patients and 12 controls at C4, in 4 patients and 13 controls at C5, in 4 patients and 14 controls at C6, in 1 patient and 7 controls at C7, and in none at C8.

The mean CSA of the whole spinal cord was smaller in patients, although this was not statistically significant ($p > .1$). The largest difference was found at segment C7 (mean difference: 8.3 mm^2) (Fig. 3A). There were no significant differences in the grey or white matter CSA between patients and controls ($p > .1$) (Fig. 3C–D). Spinal cord atrophy of the whole spinal cord ranged from 2.7% at segment C8 to 8.5% at segment C7 (Fig. 3B).

3.2.2. Microstructural properties of the cervical spinal cord

DTI scans had sufficient data quality and did not contain artifacts that could interfere with the analysis. Grey matter AD was significantly higher in patients compared to controls ($p = .03$). The largest difference was found at segment C7 (mean difference $-0.125 * 10^{-3}$ mm^2/s) (Fig. 4). There were no significant differences between patients and controls in FA, MD and RD ($p > .08$) in grey matter or white matter separately or in grey and white matter combined. There were no correlations between grey matter AD and HFMSE scores.

3.3. Cervical nerve roots

3.3.1. Thickness of the ventral and dorsal nerve roots

Mean thickness of ventral nerve roots (C4-C8) was 0.93 ± 0.13 mm in patients and 1.05 ± 0.27 mm in controls. Mean thickness of dorsal nerve roots overall, was 1.03 ± 0.22 mm in patients and 1.12 ± 0.35 mm in controls. Missing data (patients: 62.5%; controls: 45.5%) precluded meaningful statistical analysis.

3.3.2. Microstructural properties of the cervical peripheral nerve roots

DTI scans had sufficient data quality and did not contain artifacts that interfered with the analysis. Cervical nerve roots could be reconstructed with FT in 357 of 360 nerve roots. FT images of 5 SMA patients and 5 healthy controls are depicted in Fig. 5. Fig. 6 shows the diffusion parameters per segment for both patients and controls. At spinal segments C4-C8, FA was slightly lower in patients compared to controls ($p > .09$) and overall (spinal segments C3-C8) MD, AD and RD were significantly lower in patients ($p = .044$, $p = .042$ and $p = .039$ respectively). The largest differences were found at segments C3-C5: with mean differences for MD of $0.117 * 10^{-3}$ mm^2/s (C3), $0.099 * 10^{-3}$ mm^2/s (C4) and $0.133 * 10^{-3}$ mm^2/s (C5); mean differences for AD of $0.145 * 10^{-3}$ mm^2/s (C3), $0.154 * 10^{-3}$ mm^2/s (C4) and $0.207 * 10^{-3}$ mm^2/s (C5); and mean differences for RD of

Table 2
Participant characteristics.

	SMA	SMA type 2	SMA type 3a	SMA type 3b	Healthy controls
	($n = 10$)	($n = 1$)	($n = 4$)	($n = 5$)	($n = 20$)
Gender, male	6 (60%)	1	3 (75%)	3 (60%)	10 (50%)
Age, y, median (range)	52.9 (17.4–73.6)	71.6	42.9 (17.4–57.8)	51.7 (27.7–73.6)	53.9 (18.1–72.2)
mean MRC upper extremity[a], mean (SD)	3.5 (± 1.1)	2.2	3.1 (± 1.1)	4 (± 0.9)	5
mean MRC C5[b], mean (SD)	3.1 (± 1.4)	1.3	2.8 (± 1.6)	3.8 (± 1)	5
mean MRC C6[c], mean (SD)	3.9 (± 1.2)	2.3	3.4 (± 1.5)	4.5 (± 0.5)	5
mean MRC C7[d], mean (SD)	3.6 (± 1)	2.7	3.3 (± 1.1)	4.1 (± 0.8)	5
mean MRC C8[e], mean (SD)	4 (± 0.7)	3.3	3.6 (± 0.5)	4.4 (± 0.7)	5
HFMSE score, mean (SD)	25.9 (± 22.3)	4	18.8 (± 17.3)	38.5 (± 24.1)	66
FVC in sitting position, %, median (range)	91 (49–119)	65	84 (49–93)	109 (74–119)	106 (73–116)
FVC in supine position, %, median (range)	94 (67–120)	53	84 (67–97)	105 (77–120)	102 (71–115)
SMN2 copy number	4 6	1	2 2	1 4	na na

Abbreviations: SMA = spinal muscular atrophy; y = years; MRC = Medical Research Council score (range 1–5); SD = standard deviation; HFMSE = Hammersmith functional motor scale expanded; FVC = forced vital capacity; SMN = survival motor neuron; na = not applicable

[a] cervical spinal cord innervated muscles: m. supraspinatus, m. infraspinatus, deltoid muscles, m. biceps, m. triceps, m. pectoralis major, wrist flexors and extensors, finger extensors, flexors and abductors.

[b] C5 segment spinal cord innervated muscles: m. supraspinatus, m. infraspinatus, deltoid muscle, m. pectoralis major, m. biceps.

[c] C6 segment spinal cord innervated muscles: m. biceps, wrist extensors.

[d] C7 segment spinal cord innervated muscles: m. triceps, wrist extensors, finger extensors.

[e] C8 segment spinal cord innervated muscles: wrist flexors, finger flexors, finger abductors.

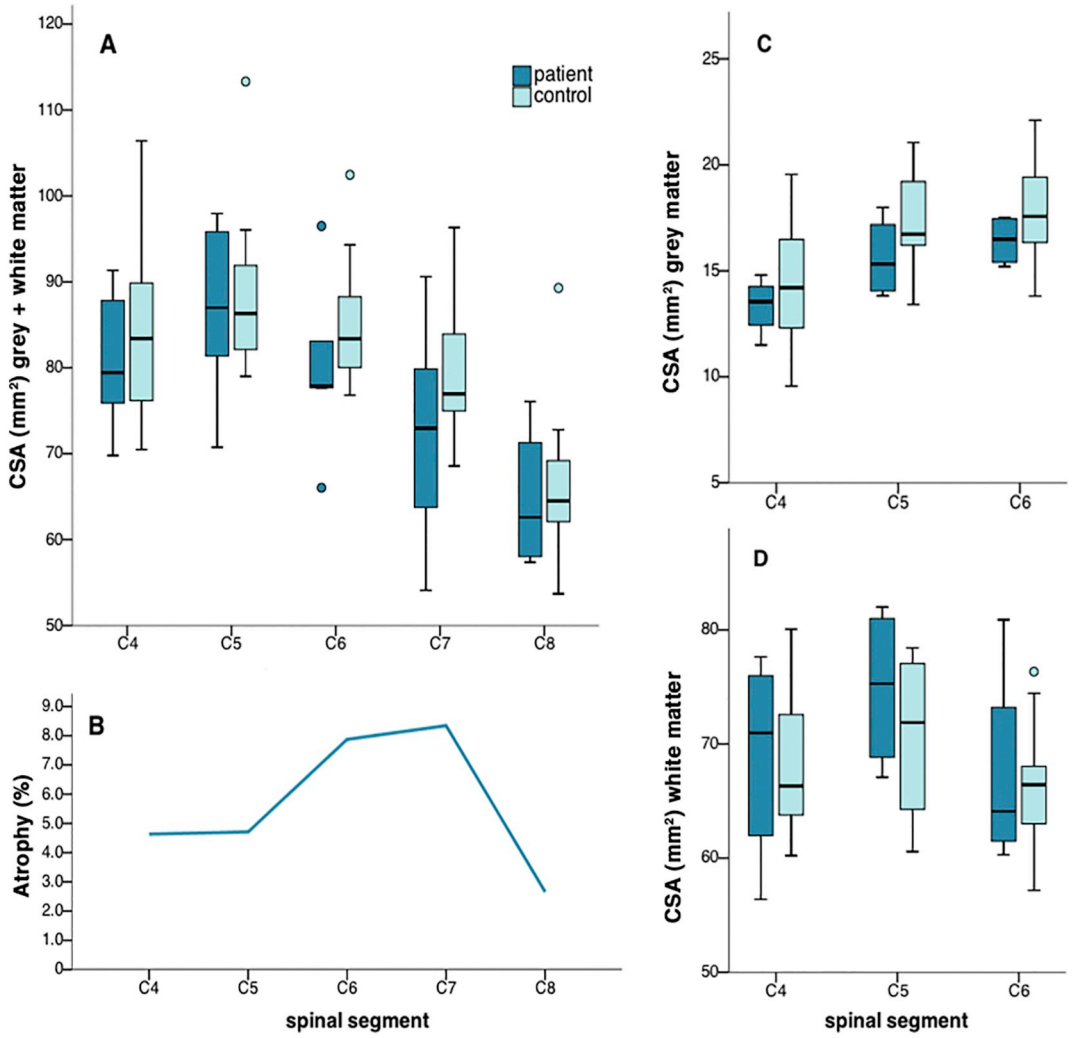

Fig. 3. Cross-sectional area of the cervical spinal cord.
Group results for SMA patients and healthy controls of CSA per spinal segment for the grey and white matter combined, A). B) Atrophy in SMA patients per spinal segment: The mean difference between patients and controls is depicted as a percentage of the control mean. CSA results of C) grey matter and D) white matter. Abbreviations: CSA = cross-sectional area; C = cervical

$0.102 * 10^{-3}\,mm^2/s$ (C3), $0.072 * 10^{-3}\,mm^2/s$ (C4) and $0.096 * 10^{-3}\,mm^2/s$ (C5). There were no correlations of any of the significant parameters with HFMSE score.

4. Discussion and conclusions

In this study we investigated the feasibility of various innovative MRI techniques to image the cervical spinal cord and nerve roots in SMA. We developed and applied 2 anatomical MRI sequences, which seem promising for future use. Additionally, we developed and applied 2 DTI sequences to investigate changes in the cervical spinal cord and nerve roots, the latter for the first time in SMA patients. We show that DTI parameters can provide important new insights into the pathology of the spinal cord and nerve roots in SMA in vivo and could potentially be used as a unique biomarker to identify and monitor disease progression.

4.1. Spinal cord

The mFFE scan showed a smaller cervical spinal cord CSA in patients compared to controls, with the largest difference at spinal segment C7. The maximal atrophy at segment C7 corresponds to the clinical finding of severe weakness of the triceps in SMA, which are innervated by this segment (MRC and Medical Research Council, 1976; Deymeer et al., 2008; Piepers et al., 2009). The smaller CSA in patients, is in line with the expected motor neuron degeneration, especially since our results indicate that the difference was mainly caused by a difference in grey matter CSA. This is in consonance which previous MRI findings of reduced cervical grey matter CSA with white matter sparing and spinal cord atrophy up to 23% in SMA (El Mendili et al., 2016; Querin et al., 2018). The spinal cord and grey matter were manually delineated to determine CSA, which may induce bias. Automatic segmentation methods may reduce this bias. However, the application of MRI remains challenging, especially at the caudal part of the cervical spinal cord (C7-C8). In some scans, artifacts, for example due to motion, precluded reliable segmentation of grey and white matter. Motion artifacts were more common in patients and may reflect the common symptom of polymyoclonus/ tremor (Dawood and Moosa, 1983). In the caudal segments, there were susceptibility artifacts due to the air in lung tissue. Future studies should focus on developing dedicated methods with less sensitivity to motion artifacts for instance by reducing scan time. Together with findings provided by a study among ALS patients, in whom CSA changed over time and correlated with clinical scores (El Mendili et al., 2014), we expect that the mFFE is a promising technique to evaluate the spinal cord in SMA.

We expected to detect a lower FA with the “high in-plane”

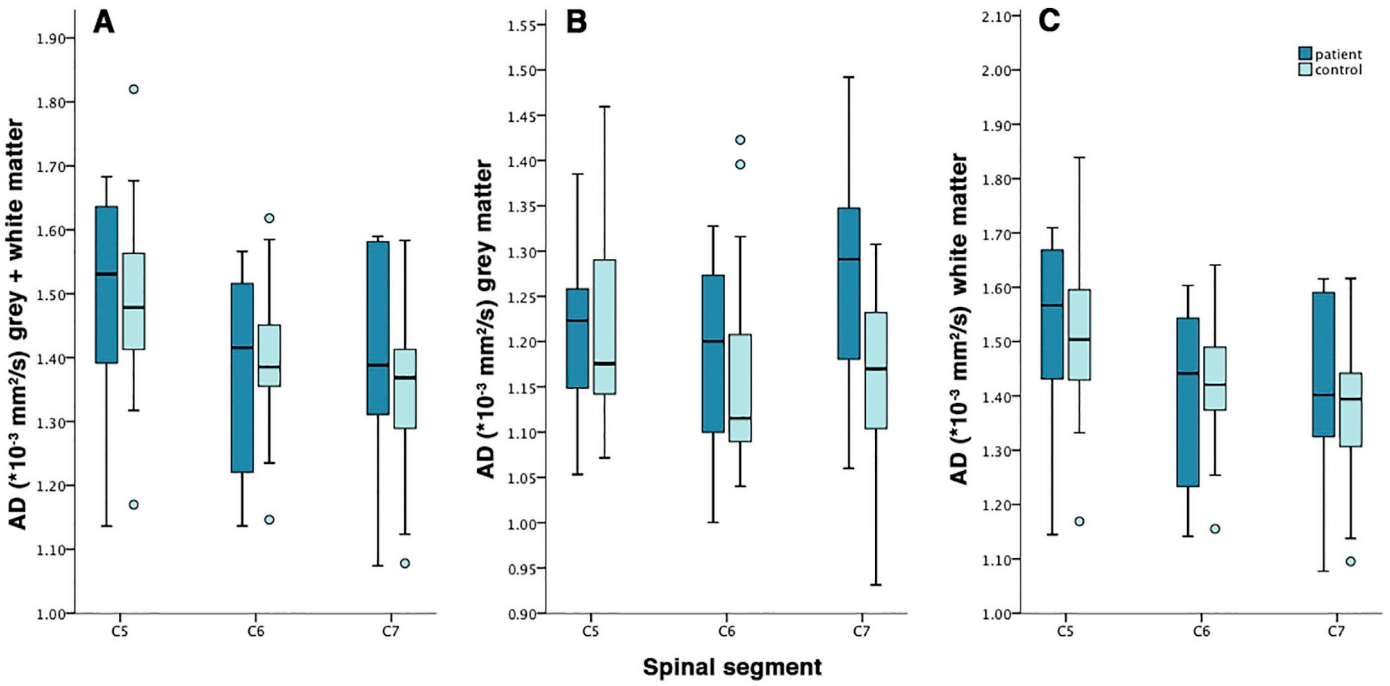

Fig. 4. Axial diffusivity values of the cervical spinal cord.
AD results per segment for SMA patients and healthy controls, in A) grey and white matter combined, B) grey matter and C) white matter.
Abbreviations: AD = axial diffusivity, C = cervical

resolution DTI scan in patients compared to healthy controls, as depletion of motor neurons may lead to an increase in extracellular space and therefore in RD, resulting in a lower FA. Instead, we detected a difference in AD, which was higher in patients compared to controls. With the mFFE scan we found that the CSA of the grey matter is smaller in SMA patients than in healthy controls. As the resolution of the "high in-plane" resolution DTI scan is only $1 \times 1\,mm^2$ in plane, partial volume effects are likely to influence the results. Moreover, smaller CSA will be more prone to these partial volume effects (Vos et al., 2011). The diffusion properties of the grey matter are in this case more influenced by the surrounding white matter, which could explain the higher AD values in patients compared to controls. This is further supported by the fact that the difference in AD is largest at segment C7, which is the segment where the CSA reduction suggested atrophy is most pronounced. Future research should therefore aim at developing MRI protocols with a higher in-plane resolution, preferably $< 0.5 \times 0.5\,mm^2$.

4.2. Cervical nerve roots

The T2-FFE scan allowed us to investigate the ventral and dorsal nerve roots. Although the patient sample size was relatively small, we observed differences in size between the ventral and dorsal nerve roots in SMA patients and healthy controls, which indicates the potential value of this technique in SMA. However, missing data were common, for both patients and healthy controls. Multiple artifacts, including local artifacts, e.g. the interference of cerebrospinal fluid at the nerve root, motion artifacts and other MR related artifacts (e.g. susceptibility artifacts), reduced scan quality. In some cases we were not able to detect the nerve despite the scan quality being otherwise good. This may occasionally be caused by reduction of the nerve root size in SMA, e.g. because of axonal abnormalities (Fallini et al., 2012; Harding et al., 2015; Araki et al., 2003; Kariya et al., 2008). However, there were also missing data in healthy controls. Future MRI protocol development should focus on reducing these artifacts.

We could reconstruct nearly all nerve roots with FT and calculate DTI parameters with the "isotropic" resolution DTI scan, which was in line with previous findings (Haakma et al., 2018). Although DTI parameters were lower in patients compared to controls at nearly all segments (C3-C8), differences in MD, AD and RD were most pronounced at the more rostral segments (C3-C5). This finding is in line with the characteristic pattern of muscle weakness in SMA, i.e. proximal muscles are usually more affected than distal muscles (Carter et al., 1995), and with previously described selective vulnerability of motor neurons and findings of cervical nerve root pathology in SMA mice (Kariya et al., 2008). Interestingly, differences in DTI parameters at segment C7 were eminent but statistically non-significant. Based on the clinical finding of early, severe weakness of the triceps in SMA (Deymeer et al., 2008; Piepers et al., 2009) and our finding of reduced CSA at segment C7, further research with a larger sample size may be able to reveal this expected difference in SMA. Additionally, patients with a shorter disease duration should be included, since one may speculate that the pronounced difference at more rostral segments is a late disease phenomenon, overshadowing the difference at segment C7. Although interpreting changes in DTI parameters in terms of pathological, microstructural changes remains challenging, abnormal DTI values could be explained by a range of SMA-associated anatomical and functional changes. Lower AD values may be associated with reduced diffusion in the length of the axon (DeBoy et al., 2007), such as lowered axonal transport in SMA (Fallini et al., 2012; Dale et al., 2011) or it may reflect the axonal degeneration that is found in SMA (Kuru et al., 2009; Ghatak, 1983). Reduced RD may be explained by glial bundles that are frequently described in nerve root pathology in SMA. One may expect an increased RD because of axonal degeneration in SMA, leading to increased intracellular space. However, in early post-mortem pathological studies of SMA nerve roots, glial bundles were seen to fill up the spaces of degenerated axons (Ghatak, 1983; Kuru et al., 2009). So, although, located outside of the myelin sheet, one may reason that the glial bundles, still inside the perineurium, will in this way limit the diffusion of water molecules perpendicular to the axon. In addition, compaction of remaining axons in the thinner ventral nerve roots of SMA patients (Harding et al., 2015; Araki et al., 2003) may represent another cause of reduced RD. As a consequence of decreased AD and RD, MD is also reduced.

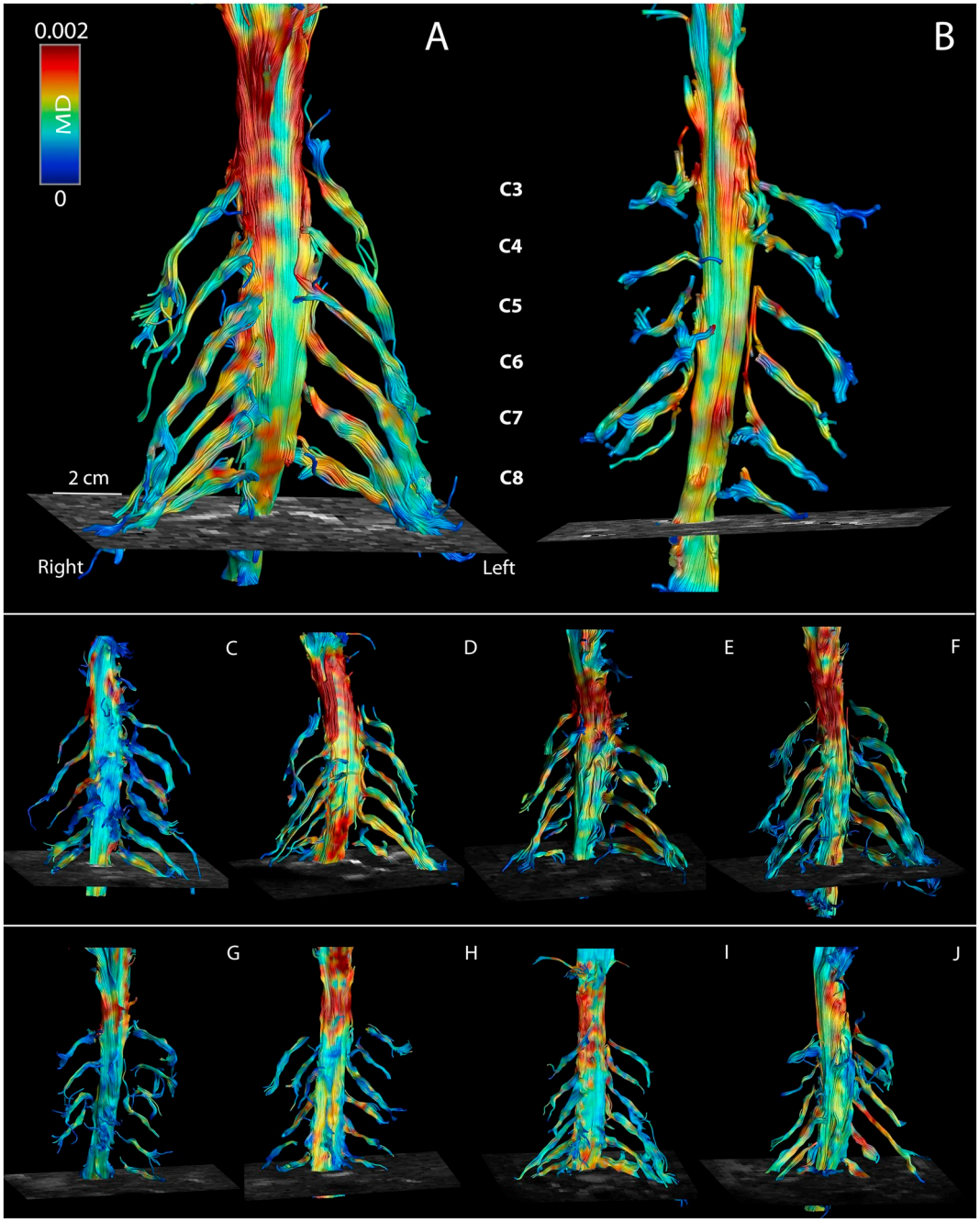

Fig. 5. Fiber tractography.
Fiber tractography images of five randomly chosen SMA patients (B, G, H, I, J) and five healthy controls (A, C, D, E, F).

The diffusion measures of the cervical nerve roots in healthy controls were lower than previously reported (Tagliafico et al., 2011). A factor known to influence FA is the signal-to-noise ratio (SNR), as with lower SNR levels, lower FA values are usually overestimated (Froeling et al., 2013). A factor influencing MD is the partial volume effects of surrounding muscular tissue and cerebral spinal fluid. These structures have a higher MD than nervous tissue which may result in the undesirable effect of higher MD estimates in nervous tissue (Schlaffke et al., 2017). From this, we infer that the lower FA and MD levels found in this study suggest that the data quality was good. The "isotropic" resolution DTI scan allowed the distinction between patients and controls. We believe this represents a promising method to evaluate in vivo (changes in) nerve microstructure in SMA.

An obvious limitation of this study is the small sample size, which affects its power. It is clear that additional, longitudinal research in larger groups is necessary to confirm our findings and to evaluate biomarker potential. Additionally, further development of MRI protocols should address the sensitivity to motion artifacts. These were most apparent in the mFFE and T2-FFE sequences in this study, influencing analysis and interpretation of the data. Shortening of scanning time could significantly reduce these motion artifacts. Novel techniques like simultaneous multislice imaging (SMS) (Barth et al., 2016), using parallel image reconstruction, or compressed sensing (CS) (Hollingsworth, 2015), based on acquiring only data of a small amount of (target) pixels, could potentially be implemented to accelerate data acquisition. In the future, it would be interesting also to investigate the lumbar spinal cord with DTI, since lower limbs are usually more affected than upper limbs in SMA. However, the application of DTI in the lower

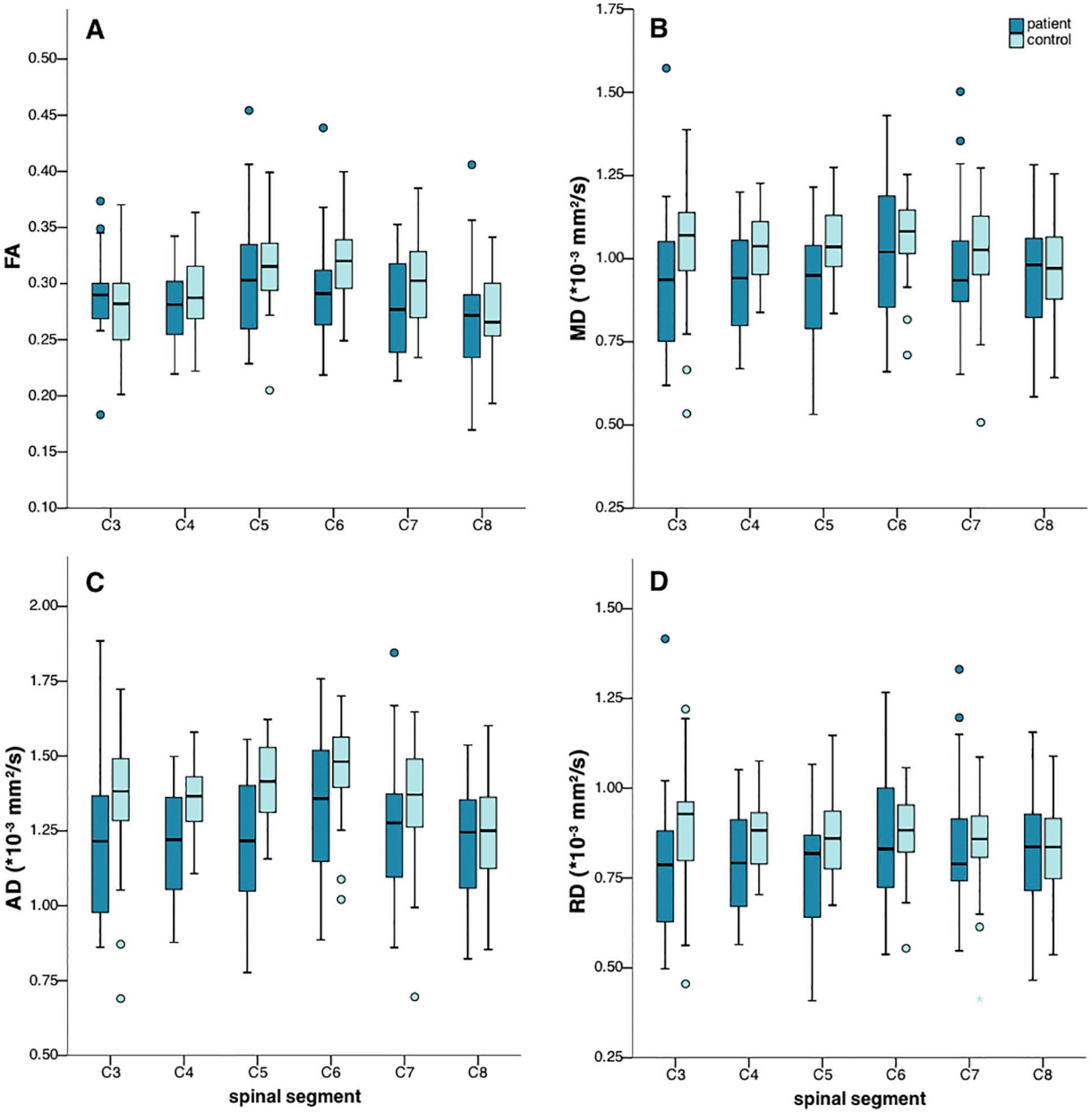

Fig. 6. Microstructural properties of the cervical peripheral nerve roots.
Group results for SMA patients and healthy controls of the DTI parameters A) fractional anisotropy (FA), B) mean (MD), C) axial (AD) and D) radial diffusivity (RD) for nerve roots at each cervical spinal segment.

thoracic and higher lumbar spinal cord to investigate grey and white matter is currently still challenging due to several technical issues, such as the presence of susceptibility artifacts caused by the air in lung tissue. Finally, a factor to be considered in clinical application of these techniques are the, non-disease-related changes in MRI/DTI metrics of the spinal cord during ageing, for which the availability of reference values are currently still limited (Taso et al., 2016). In this study we adjusted for age in the study design, by including age-matched healthy controls to our patient population.

To summarize, we have developed 4 MRI sequences that provide measures of both anatomical and structural changes in SMA. The results suggest that, when further developed, MRI and DTI might provide unique anatomical and functional biomarkers to monitor SMA progression and treatment effects.

Author contributions

Study concept and design: MS, WH, MF, LAMO, LHB, JH, WLP. Data acquisition, analysis and/or interpretation of data: MS, WH, LK, MF, MEP, CB, AL, JH, WLP. Drafting of the manuscript: MS, WH. Critical revision of manuscript: MS, WH, LK, MF, MEP, CB, AL, LAMO, LHB, JH, WLP.

Declaration of Competing Interests

Leonard H. van den Berg serves on scientific advisory boards for the Prinses Beatrix Spierfonds, Thierry Latran Foundation, Biogen Idec and Cytokinetics; received an educational grant from Baxter International Inc.; serves on the editorial board of Amyotrophic Lateral Sclerosis and the Journal of Neurology, Neurosurgery and Psychiatry; and receives research support from the Prinses Beatrix Fonds.

W. Ludo van der Pol serves on scientific advisory boards of Biogen and Avexis and the LMI070 data monitoring committee of Novartis and receives research support from the Prinses Beatrix Spierfonds, Netherlands ALS Foundation and Stichting Spieren voor Spieren.

Marloes Stam, Wieke Haakma, Lidy Kuster, Martijn Froeling, Marielle E.P. Philippens, Clemens Bos, Alexander Leemans, Louise A.M. Otto and Jeroen Hendrikse report no competing interest.

Funding

This study was supported by grants from the Prinses Beatrix Spierfonds (WAR08-24, WAR13-07 and WAR14-26) and Stichting Spieren voor Spieren. Prinses Beatrix Spierfonds and Stichting Spieren voor Spieren had no role in study design, data collection, data analysis or interpretation, writing the report or decisions concerning submitting this paper.

Acknowledgements

The authors thank all patients and healthy controls who participated in this study. We would also like to thank Mrs. Bea Nijboer for her contribution in data collection, Mr. Stavros Nikolakopoulos for his statistical advice, and Tuan Nguyen and Ellart Aalbers for their help in acquiring the images.

References

Araki, S., Hayashi, M., Tamagawa, K., et al., 2003. Neuropathological analysis in spinal muscular atrophy type II. Acta Neuropathol. 106 (5), 441–448.

Barth, M., Breuer, F., Koopmans, P.J., et al., 2016. Simultaneous multislice (SMS) imaging techniques. Magn. Reson. Med. 75 (1), 63–81. https://doi.org/10.1002/mrm.25897.

Bertini, E., Burghes, A., Bushby, K., et al., 2005. 134th ENMC international workshop: outcome measures and treatment of spinal muscular atrophy 11-13 February 2005 Naarden, the Netherlands. Neuromuscul. Disord. 15 (11), 802–816.

Carter, G.T., Abresch, R.T., Fowler, W.M., et al., 1995. Profiles of neuromuscular diseases. Spinal muscular atrophy. Am. J. Phys. Med. Rehabil. 74 (5 Suppl), S150–S159.

Dale, J.M., Shen, H., Barry, D.M., et al., 2011. The spinal muscular atrophy mouse model, SMAΔ7, displays altered axonal transport without global neurofilament alterations. Acta Neuropathol. 122 (3), 331–341.

Dawood, A.A., Moosa, A., 1983. Hand and ECG tremor in spinal muscular atrophy. Arch. Dis. Child. 58 (5), 376–378.

DeBoy, C.A., Zhang, J., Dike, S., et al., 2007. High resolution diffusion tensor imaging of axonal damage in focal inflammatory and demyelinating lesions in rat spinal cord. Brain 130 (8), 2199–2210.

Deymeer, F., Serdaroglu, P., Parman, Y., et al., 2008. Natural history of SMA IIIb: muscle strength decreases in a predictable sequence and magnitude. Neurology 71 (9), 644–649.

Durmus, H., Yilmaz, R., Gulsen-Parman, Y., et al., 2017. Muscle magnetic resonance imaging in spinal muscular atrophy type 3: selective and progressive involvement. Muscle Nerve 55 (5), 651–656.

El Mendili, M.M., Cohen-Adad, J., Pelegrini-Issac, M., et al., 2014. Multi-parametric spinal cord MRI as potential progression marker in amyotrophic lateral sclerosis. PLoS One 9 (4), e95516. Available at. https://journals.plos.org/plosone/.

El Mendili, M.M., Lenglet, T., Stojkovic, T., et al., 2016. Cervical spinal cord atrophy profile in adult SMN1-linked SMA. In: PLoS One Online, [e0152439] 18 April. 10.1371/journal.pone.0152439.

Fallini, C., Bassell, G.J., Rossoll, W., 2012. Spinal muscular atrophy: the role of SMN in axonal mRNA regulation. Brain Res. 1462, 81–92.

Froeling, M., Nederveen, A.J., Nicolay, K., et al., 2013. DTI of human skeletal muscle: the effects of diffusion encoding parameters, signal-to-noise ratio and T2 on tensor indices and fiber tracts. NMR Biomed. 26 (11), 1339–1352.

Ghatak, 1983. Glial bundles in spinal nerve roots: a form of isomorphic gliosis at the junction of the central and peripheral nervous system. Neuropathol. Appl. Neurobiol. 9 (5), 391–401. https://doi.org/10.1111/j.1365-2990.1983.tb00124.x.

Haakma, W., Pedersen, M., Froeling, M., et al., 2016. Diffusion tensor imaging of peripheral nerves in non-fixed post-mortem subjects. Forensic Sci. Int. 263, 139–146.

Haakma, W., Jongbloed, B.A., Froeling, M., et al., 2017. MRI shows thickening and altered diffusion in the median and ulnar nerves in multifocal motor neuropathy. Eur. Radiol. 27 (5), 2216–2224.

Haakma, W., Froeling, M., Pedersen, M., et al., 2018. Post-mortem diffusion MRI of the cervical spine and its nerve roots. J. Forensic Radiol. Imaging 12, 50–56.

Harding, B.N., Kariya, S., Monani, U.R., et al., 2015. Spectrum of neuropathophysiology in spinal muscular atrophy type I. J. Neuropathol. Exp. Neurol. 74 (1), 15–24.

Hollingsworth, K.G., 2015. Reducing acquisition time in clinical MRI by data undersampling and compressed sensing reconstruction. Phys. Med. Biol. 7 (60(21)), R297–R322. https://doi.org/10.1088/0031-9155/60/21/R297.

Irfanoglu, M.O., Walker, L., Sarlls, J., et al., 2012. Effects of image distortions originating from susceptibility variations and concomitant fields on diffusion MRI tractography results. Neuroimage 61 (1), 275–288.

Kariya, S., Park, G.H., Maeno-Hikichi, Y., et al., 2008. Reduced SMN protein impairs maturation of the neuromuscular junctions in mouse models of spinal muscular atrophy. Hum. Mol. Genet. 17 (16), 2552–2569.

Kuru, S., Sakai, M., Konagaya, M., et al., 2009. An autopsy case of spinal muscular atrophy type III (Kugelberg-Welander disease). Neuropathology 29 (1), 63–67.

Leemans, A., Jones, D.K., 2009. The B-matrix must be rotated when correcting for subject motion in DTI data. Magn. Reson. Med. 61 (6), 1336–1349 (b).

Leemans, A., Jeurissen, B., Sijbers, J., et al., 2009. ExploreDTI: a graphical toolbox for processing, analyzing, and visualizing diffusion MR data. In: Presented at the 17th Scientific Meeting of the International Society for Magnetic Resonance in Medicine. May 18–25, 2009 Honolulu. 17 (2):3537 (a).

Lunn, M.R., Wang, C.H., 2008. Spinal muscular atrophy. Lancet 371 (9630), 2120–2133.

MRC, Medical Research Council, 1976. Aids to the Examination of the Peripheral Nervous System: Memorandum no 45 (Suspending War Memorandum No. 7). London. .

Müller, H.P., Turner, M.R., Grosskreutz, J., et al., 2016. A large-scale multicentre cerebral diffusion tensor imaging study in amyotrophic lateral sclerosis. J. Neurol. Neurosurg. Psychiatry 87 (6), 570–579.

Munsat, T.L., Davies, K.E., 1992. International SMA consortium meeting (26-28 June 1992, Bonn, Germany). Neuromuscul. Disord. 2 (5–6), 423–428.

O'Hagen, J.M., Glanzman, A.M., McDermott, M.P., et al., 2007. An expanded version of the Hammersmith functional motor scale for SMA II and III patients. Neuromuscul. Disord. 17 (9–10), 693–697.

Oudeman, J., Nederveen, A.J., Strijkers, G.J., et al., 2016. Techniques and applications of skeletal muscle diffusion tensor imaging: a review. J. Magn. Reson. Imaging 43 (4), 773–788.

Pellizzoni, L., Kataoka, N., Charroux, B., et al., 1998. A novel function for SMN, the spinal muscular atrophy disease gene product, in pre-mRNA splicing. Cell 95 (5), 615–624.

Piepers, S., van der Pol, W.L., Brugman, F., et al., 2009. Natural history of SMA IIIb: muscle strength decreases in a predictable sequence and magnitude. Neurology 72 (23), 2057–2058.

Querin, G., El Mendili, M.M., Lenglet, T., et al., 2018. The spinal and cerebral profile of adult spinal-muscular atrophy: a multimodal imaging study. Neuroimage Clin. https://doi.org/10.1016/j.nicl.2018.101618. Published Online First: 28 November.

Schlaffke, L., Rehmann, R., Froeling, M., et al., 2017. Diffusion tensor imaging of the human calf: variation of inter- and intramuscle-specific diffusion parameters. J. Magn. Reson. Imaging 46 (4), 1137–1148.

Sproule, D.M., Montgomery, M.J., Punyanitya, M., et al., 2011. Thigh muscle volume measured by magnetic resonance imaging is stable over a 6-month interval in spinal muscular atrophy. J. Child Neurol. 26 (10), 1252–1259.

Sumner, C.J., Crawford TO, 2018. Two breakthrough gene-targeted treatments for spinal muscular atrophy: challenges remain. J. Clin. Invest. 128 (8), 3219–3227.

Tagliafico, A., Calabrese, M., Puntoni, M., et al., 2011. Brachial plexus MR imaging: accuracy and reproducibility of DTI-derived measurements and fibre tractography at 3.0-T. Eur. Radiol. 21 (8), 1764–1771.

Taso, M., Girard, O.M., Duhamel, G., et al., 2016. Tract-specific and age-related variations of the spinal cord microstructure: a multi-parametric MRI study using diffusion tensor imaging (DTI) and inhomogeneous magnetization transfer (ihMT). NMR Biomed. 29 (6), 817–832. https://doi.org/10.1002/nbm.3530.

Toosy, A.T., Kou, N., Altmann, D., et al., 2014. Voxel-based cervical spinal cord mapping of diffusion abnormalities in MS-related myelitis. Neurology 83 (15), 1321–1325.

Tournier, J.D., Mori, S., Leemans, A., 2011. Diffusion tensor imaging and beyond. Magn. Reson. Med. 65 (6), 1532–1556.

Veraart, J., Sijbers, J., Sunaert, S., et al., 2013. Weighted linear least squares estimation of diffusion MRI parameters: strengths, limitations, and pitfalls. Neuroimage 81 (0), 335–346.

Vos, S.B., Jones, D.K., Viergever, M.A., et al., 2011. Partial volume effect as a hidden covariate in DTI analyses. Neuroimage 55 (4), 1566–1576.

Wadman, R.I., Stam, M., Gijzen, M., et al., 2017. Association of motor milestones, SMN2 copy and outcome in spinal muscular atrophy types 0-4. J. Neurol. Neurosurg. Psychiatry 88 (4), 364–367.

Zerres, K., Schöneborn, S.R., 1995. Natural history in proximal spinal muscular atrophy: clinical analysis of 445 patients and suggestions for a modification of existing classifications. Arch. Neurol. 52 (5), 518–523.